

Multiphysics metamirrors for simultaneous manipulations of acoustic and electromagnetic waves

Ana Díaz-Rubio and Sergei Tretyakov

Department of Electronics and Nanoengineering, Aalto University, P. O. Box 15500, FI-00076 Aalto, Finland

Metasurfaces have shown unprecedented possibilities for wavefront manipulation of waves. The research efforts have been focused on the development of metasurfaces that perform a specific functionality for waves of one physical nature, for example, for electromagnetic waves. In this work, we propose the use of power-flow conformal metamirrors for creation of multiphysics devices which can simultaneously control waves of different nature. In particular, we introduce metasurface devices which perform specified operations on both electromagnetic and acoustic waves at the same time. Using a purely analytical model based on surface impedances, we introduce metasurfaces that perform the same functionality for electromagnetic and acoustic waves and, even more challenging, different functionalities for electromagnetics and acoustics. We provide realistic topologies for practical implementations of proposed metasurfaces and confirm the results with numerical simulations.

I. INTRODUCTION

Over the last few years, great efforts have been concentrated on studying new possibilities for controlling wave propagation using microstructured surfaces, so-called metasurfaces. Research on metasurfaces covers aspects from the theory of wave propagation, fabrication techniques, and even different disciplines or application fields such as acoustics [1] or electromagnetism [2] [3]. Metasurfaces have shown great potential for manipulating waves both in transmission and reflection. In particular, metasurfaces controlling reflection, also known as metamirrors, have been developed for realizations of retroreflectors, anomalous reflectors, beam splitters, and focusing devices [4–13].

In the design of reflective metasurfaces, one can distinguish two different types of design strategies. On the one hand, there are examples of several *non-local design approaches* where the properties on each point of the metasurface depend not only on the local field at this specific point but also on the fields in the vicinity of this point [5–7, 10, 11, 14]. Exploiting non-locality it is possible to reduce the number of meta-atoms required for the implementation. However, the corresponding design approaches are complicated especially for complex functionalities such as focusing. On the other hand, using *local design approaches* the properties of the metasurface at each point can be uniquely characterized by response on the local fields at this point [8, 12, 13]. In this case, the metasurface can be characterized by local parameters such as the surface impedance. The main advantage of these methods is that knowing the desired performance of the metasurface, the design of metasurfaces becomes systematic and in most of the cases it does not require numerical optimizations. In recent work [12] it was demonstrated that local design of metasurfaces is possible by proper engineering the shape and the surface impedance according to the power-flow distribution of the required set of waves.

In this work, we will show that exploiting the properties of local metasurfaces one can design multiphysics

devices which can simultaneously control waves of different nature. This becomes possible because power flow-conformal metasurfaces can be realized as arrays of small (subwavelength) meta-atoms acting as phase-shifting elements [12]. Here we exploit a possibility to create meta-atoms which can provide controllable phase shifts for both electromagnetic waves and for sound, which open up a way towards creation of high-performance multi-functional multi-physics metasurface devices.

Although acoustic and electromagnetic waves obey different wave propagation equations that, respectively, govern sound pressure and electromagnetic field distributions, there exists a direct analogy that allows to create multi-physics structures [15]. In particular, we study the analogy of impedance-based models for electromagnetic and acoustic reflectors. In this paper, we exploit this analogy and present a direct and comparative approach for the design and implementation of power flow-conformal metamirrors for both acoustic and electromagnetic fields. We demonstrate that using power

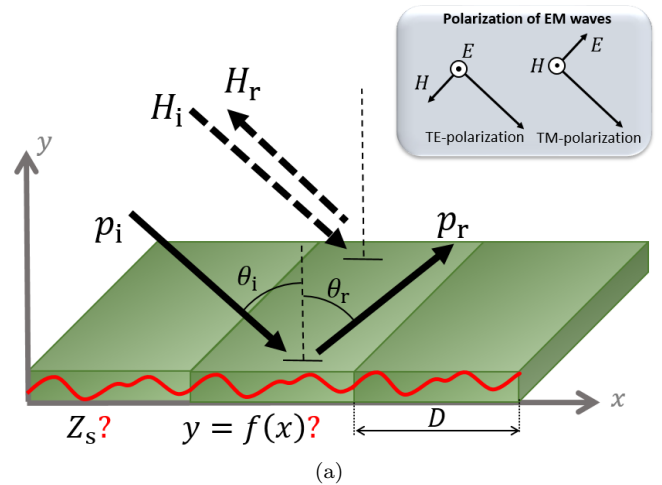


FIG. 1. Schematic representation of a multiphysics metamirror.

flow-conformal metamirrors and the local-parameter approach, the design of such multiphysics devices becomes systematic and straightforward. Several example functionalities are analyzed and characterized in terms of the shape and surface impedance of the metamirror, as well as topologies of physical implementations. The study shows similarities and differences between both wave problems (acoustic and electromagnetic) that have to be considered in the final implementation of multiphysics platforms.

The paper is organized as follows. First, in Section II, we present the theory for the design of power flow-conformal metamirrors paying special attention to the similarities and differences between the two domains of physics. In particular, the study will be focused on manipulation of two plane waves (retroreflectors and anomalous reflectors). This allows us to streamline the design of metamirrors that allow simultaneous control of both acoustic and electromagnetic responses. Next, in Section III, we discuss practical aspects related to actual implementations of multi-physics metamirrors. Finally, some conclusions summarize the main findings of this work.

II. GENERAL THEORETICAL FRAMEWORK

In this section, we present the theory of power flow-conformal metamirrors and highlight the differences between acoustic and electromagnetic devices for shaping reflected waves. More specifically, we will discuss the design of reflective surfaces for reflecting an incident plane wave into a desired direction. The key parameter to be considered in the solutions of both problems is the surface impedance, which can be defined for both electromagnetic and acoustic waves.

Let us consider a curved impenetrable boundary lying on the xz -plane whose shape is defined by the function $y_c = f(x)$ (for simplicity we assume that the surface profile is uniform along the orthogonal direction z). For acoustic waves, the surface impedance $Z_s(x)$ is defined as a relation between the pressure p and velocity \mathbf{v} fields: $Z_s(x)\hat{\mathbf{n}} \cdot \mathbf{v}(x, y_c) = -p(x, y_c)$. Here, $\hat{\mathbf{n}}$ is the unit vector normal to the surface of the metamirror at point x . For electromagnetic waves, the surface impedance is defined as a relation between the tangential to the surface components of the electric and magnetic fields, \mathbf{E}_t and \mathbf{H}_t , as $Z_s(x)\hat{\mathbf{n}} \times \mathbf{H}_t(x, y_c) = \mathbf{E}_t(x, y_c)$.

The wave fields above a perfect anomalously reflecting metamirror are sums of fields of only two plane waves: one is the incident plane wave and the other is the reflected plane wave, which propagates in the desired, freely chosen direction. In order to find the optimal surface profile, $y_c = g(x)$, which ensures the desired functionalities of the metamirror, the first step is to analyze the distribution of power flow in this set of two plane waves [12]. In what follows, we will analyse the power flow for both electromagnetic and acoustic problems.

Acoustic metamirror: The wave vectors of the waves can be defined as $\mathbf{k}_{i,r} = k_{i,r}^{(x)}\hat{\mathbf{x}} + k_{i,r}^{(y)}\hat{\mathbf{y}}$, where the subscript $i(r)$ denotes the incident (reflected) plane wave. In the most general case, we can define the incident wavevector as $\mathbf{k}_i = k(\sin\theta_i\hat{\mathbf{x}} - \cos\theta_i\hat{\mathbf{y}})$, where θ_i is the incident angle (anti-clockwise definition) and $k = \omega/c_{ac}$ is the wavenumber of sound waves in the background medium at the frequency of interest (c_{ac} is the speed of sound). Following the same notation, the wavevector of the reflected wave is defined as $\mathbf{k}_r = k(\sin\theta_r\hat{\mathbf{x}} + \cos\theta_r\hat{\mathbf{y}})$ with θ_r being the reflection angle (clockwise definition). A schematic representation of this scenario is shown in Fig. 1. Under the $e^{j\omega t}$ time convention, the field can be expressed as follows:

$$p(x, y) = p_i e^{-j\mathbf{k}_i \cdot \mathbf{r}} + p_r e^{-j\mathbf{k}_r \cdot \mathbf{r}} \quad (1)$$

$$v_x(x, y) = \frac{1}{\omega\rho} \left[p_i k_i^{(x)} e^{-j\mathbf{k}_i \cdot \mathbf{r}} + p_r k_r^{(x)} e^{-j\mathbf{k}_r \cdot \mathbf{r}} \right] \quad (2)$$

$$v_y(x, y) = \frac{1}{\omega\rho} \left[p_i k_i^{(y)} e^{-j\mathbf{k}_i \cdot \mathbf{r}} + p_r k_r^{(y)} e^{-j\mathbf{k}_r \cdot \mathbf{r}} \right] \quad (3)$$

where $p_i = |p_i|e^{j\phi_i}$ and $p_r = |p_r|e^{j\phi_r}$ are the complex amplitudes of the incident and reflected plane waves, $\mathbf{r} = x\hat{\mathbf{x}} + y\hat{\mathbf{y}}$ is the position vector, ω is the angular frequency, and ρ is the density of the background media. From the definition of the pressure and velocity vector, it is straightforward to derive the intensity vector of the superposition of both incident and reflected plane waves as $\mathbf{I}(x, y) = \frac{1}{2}\text{Re}(p\mathbf{v}^*) = I_x(x, y)\hat{\mathbf{x}} + I_y(x, y)\hat{\mathbf{y}}$. The analytical expression of the flow of power carried by two arbitrary plane waves reads

$$I_x(x, y) = I_0 \left[|p_i|^2 k_i^{(x)} + |p_r|^2 k_r^{(x)} \right] + I_0 |p_i| |p_r| (k_i^{(x)} + k_r^{(x)}) \cos(\Delta\mathbf{k} \cdot \mathbf{r} + \Delta\phi) \quad (4)$$

and

$$I_y(x, y) = I_0 \left[|p_i|^2 k_i^{(y)} + |p_r|^2 k_r^{(y)} \right] + I_0 \left[|p_i| |p_r| (k_i^{(y)} + k_r^{(y)}) \cos(\Delta\mathbf{k} \cdot \mathbf{r} + \Delta\phi) \right], \quad (5)$$

where $I_0 = 1/2\omega\rho$, $\Delta\mathbf{k} = \mathbf{k}_r - \mathbf{k}_i$, and $\Delta\phi = \phi_i - \phi_r$.

Electromagnetic metamirror: The analysis of the power-flow distribution for electromagnetic waves can be done following a similar approach. Because of the vectorial nature of the problem, here we should distinguish between TM-polarized (H_z , E_x , and E_y) and TE-polarized (E_z , H_x , and H_y) waves. Notice that in this work we do not consider any change in the polarization state and assume that both incident and reflected waves have the same polarization. As it was shown in [12], the power-flow distribution in the electromagnetic counterpart defined by the Poynting vector $\mathbf{S} = \frac{1}{2}\text{Re}(\mathbf{E} \times \mathbf{H}^*) = S_x(x, y)\hat{\mathbf{x}} + S_y(x, y)\hat{\mathbf{y}}$ is given by similar expressions as in Eqs. (4) and (5). There is a clear analogy between the two physical problems: For TM-polarized waves, the amplitude of the pressure

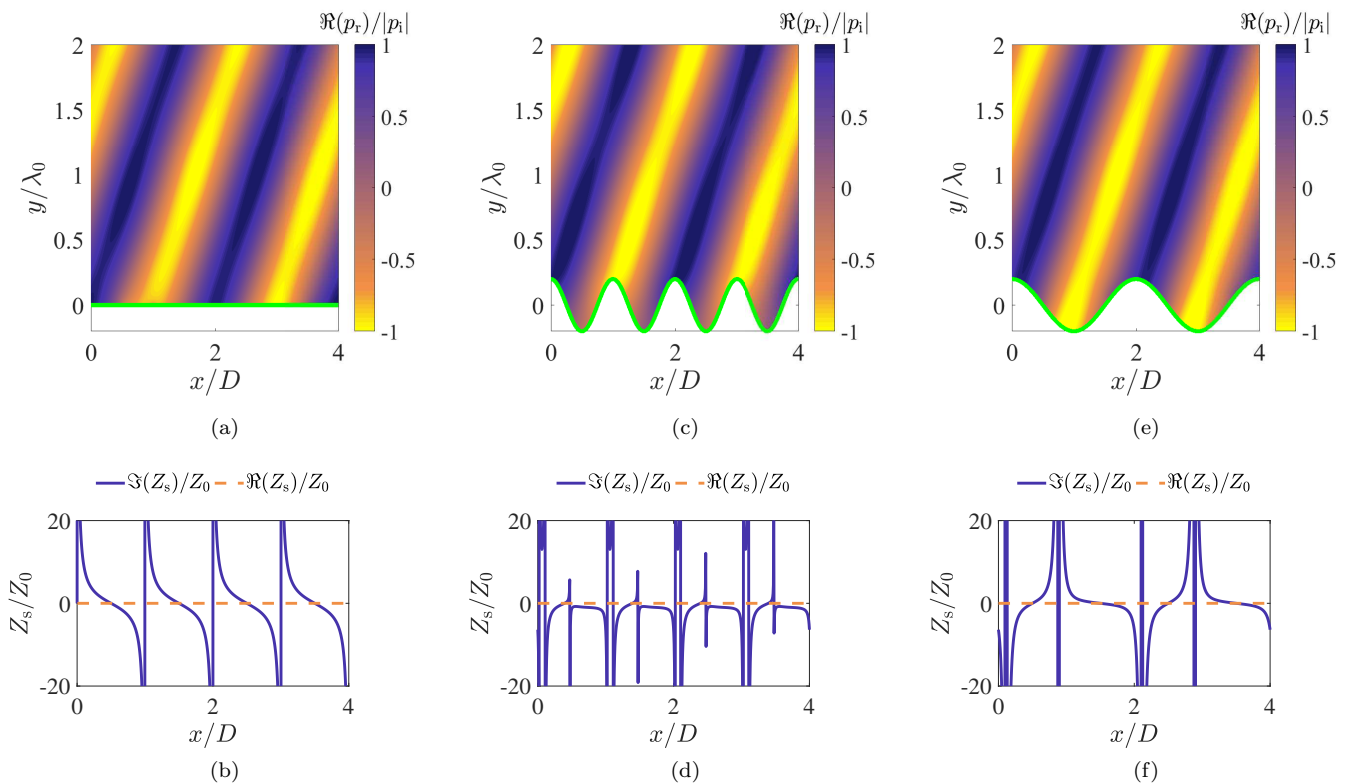


FIG. 2. Acoustic power flow-conformal retroreflectors for $\theta_i = 70^\circ$. Reflected pressure field (a) and normalized surface impedance (b) for the flat retroreflector. Reflected pressure field (c) and normalized surface impedance (d) for the retroreflector with cosine profile $y_c = \frac{\lambda}{5} \cos(2\pi x/D)$. Reflected pressure field (e) and normalized surface impedance (f) for the retroreflector with cosine profile $y_c = \frac{\lambda}{5} \cos(\pi x/D)$.

fields is analogous to the amplitude of magnetic fields ($p_{i,r} \rightarrow H_{i,r}$) and the density of the background media to the permittivity ($\rho \rightarrow \varepsilon_0$). For TE-polarized waves the amplitude of electric fields plays the role of the amplitude of the pressure fields ($p_{i,r} \rightarrow E_{i,r}$) and the density of the background media is analogous to the permeability ($\rho \rightarrow \mu_0$).

From the analysis of the power-flow density distribution we can see that the power-flow distribution mainly depends on the amplitude of the plane waves ($|p_i|$ and $|p_r|$) and the direction of propagation (\mathbf{k}_i and \mathbf{k}_r). We can distinguish three different scenarios depending on the relations between these parameters: (i) When $|p_i| = |p_r|$ and $\mathbf{k}_r = -\mathbf{k}_i$, the wave is reflected back towards the source, and we call it the retroreflection scenario. (ii) Reflections with $|p_i| = |p_r|$ but $\mathbf{k}_r \neq -\mathbf{k}_i$ can be realized if the wave reflects specularly. (iii) Finally, full power reflection is possible with $|p_i| \neq |p_r|$ and $\mathbf{k}_r \neq \mathbf{k}_i$. This case is usually called anomalous reflection. In the following, we will consider in detail multiphysics realizations of all these scenarios.

A. Retroreflection

The first case under study is the retroreflection scenario, i.e., we study surfaces capable of redirecting all the energy of an incident plane wave into the opposite direction ($\mathbf{k}_r = -\mathbf{k}_i$), back to the source. First, we will analyse acoustic retroreflectors. In order to warranty the power conservation, the amplitudes of incident and reflected waves should be equal, $|p_i| = |p_r|$. By substituting these values in Eqs. 4 and 5, we can see that the intensity power-flow vector is zero at all points of space, $I_x(x, y) = I_y(x, y) = 0$. It means that in this special case we can design local retroreflectors with any shape, as the power will never cross the reflector boundary.

Figure 2 shows three different retroreflectors designed for $\theta_i = 70^\circ$. The first example corresponds to a flat retroreflector where the surface profile is defined as $y_c = 0$. Figure 2(b) shows the required normalized surface impedance. In the acoustic case, the impedance is normalized with respect to $Z_0 = Z_0^{\text{ac}} = c_{\text{ac}}\rho$. The surface impedance function defines the period of the reflector that reads $D = \lambda/(2 \sin \theta_i)$. Results of numerical simulations of the reflected pressure field are shown in Fig. 2(a) where we can see the reflected plane wave propagating into the opposite direction with respect to that of the in-

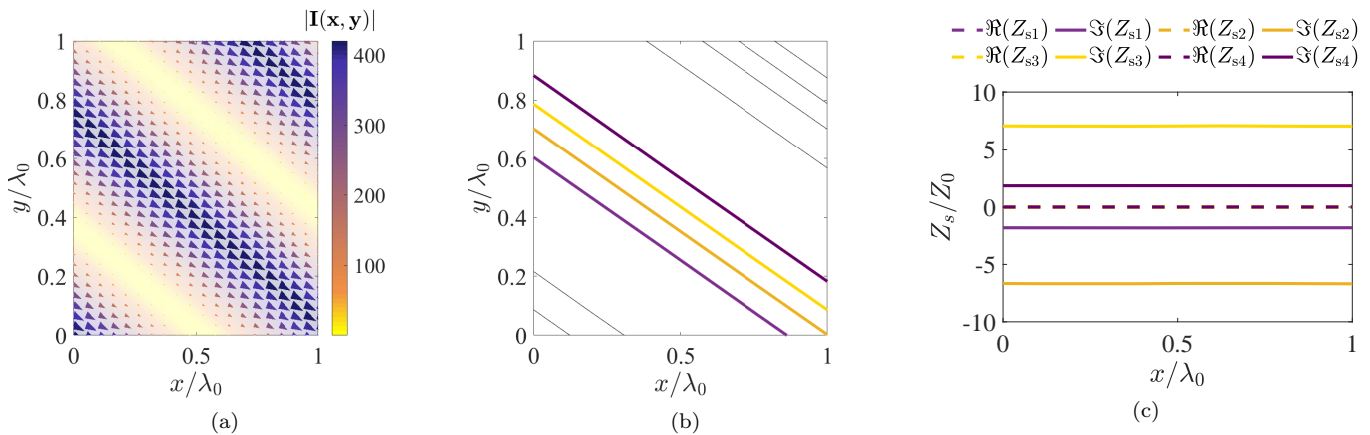


FIG. 3. Results for sets of two plane waves with $|p_i| = |p_r|$, $\theta_i = 0^\circ$, and $\theta_r = 70^\circ$. (a) Power flow distribution. (b) Set of surfaces tangential to the intensity vector and (c) the corresponding surface impedance associated with each surface. The four surfaces are denoted by subscripts 1,2,3, and 4.

cident plane wave. The second example is a retroreflector with a cosine surface profile $y_c = \frac{\lambda}{5} \cos(2\pi x/D)$ with the same period as the flat reflector. Figures 2(c) and 2(d) show the reflected field and the normalized surface impedance for this design. We can see that the surface impedance is also purely imaginary confirming the local nature of the design.

The last example is a retroreflector with a cosine modulation where the period is double of that for the flat reflector: $D' = 2D$. The curve which describes this surface modulation profile can be expressed as $y_c = \frac{\lambda}{5} \cos(\pi x/D)$. The reflected field and the corresponding surface impedance are shown in Figs. 2(e) and 2(f). It is important to mention that the spatial periodicity of the metasurface can be used as a control parameter for the diffracted modes in the system, allowing us to control reflection for illuminations from other directions.

For design of electromagnetic retroreflectors, even though the physical meaning of the surface impedance is different, we can use the mathematical analogy with the acoustic scenario. The correspondence between normalized acoustic and electromagnetic impedances for TE-polarized waves is direct: $Z_s^{ac}/Z_0^{ac} = Z_s^{TE}/Z_0^{EM}$, with $Z_0^{ac} = c_{ac}\rho$ being the acoustic wave impedance and $Z_0^{EM} = c_{EM}\mu$ the electromagnetic wave impedance. Here, c_{ac} and c_{EM} are the speed of sound and light, respectively. ρ is the mechanical density of medium. However, for TM-polarized waves we obtain, due to the duality of the problem, that $Z_s^{ac}/Z_0^{ac} = Z_0^{EM}/Z_s^{TM} = Z_0^{EM}Y_s^{TM}$. As we will show, these relations between required impedances for metamirror surfaces will define certain constraints in the design of multiphysics metamirrors.

B. Specular reflection

Next, we consider reflection into a wave with the same amplitude, $|p_i| = |p_r|$, but propagating in another direc-

tion, with $\mathbf{k}_r \neq \mathbf{k}_i$. In this case, from Eqs. (4) and (5) we can see that in general $I_x(x,y) \neq 0$ and $I_y(x,y) \neq 0$. As an example, Fig. 3(a) shows the power-flow distribution in two interfering plane waves when $\theta_i = 0^\circ$ and $\theta_r = 70^\circ$. It is clear from the analysis of the power flow that the surfaces through which there is no power flow are flat surfaces. Figure 3(b) shows a set of surfaces which are tangential to the intensity vector. The inclination angle can be written as $\theta_s = \arctan\left(\frac{-\sin\theta_i + \sin\theta_r}{\cos\theta_i + \cos\theta_r}\right)$. The components of the unit normal vector $\mathbf{n} = n_x\hat{\mathbf{x}} + n_y\hat{\mathbf{y}}$ are defined as $n_x = \frac{1}{\sqrt{2}}(\sin\theta_i + \sin\theta_r)$ and $n_y = \frac{1}{\sqrt{2}}(\cos\theta_i - \cos\theta_r)$. Clearly, these results correspond to trivial specular reflection from these flat surfaces.

The required impedances for each surface are represented in Fig. 3(c). We see that the surface impedances are purely imaginary and constant along the surfaces. Depending on the defined surface, the surface impedance takes different values to ensure the desired phase shift between the incident and reflected waves. We can find positions of surfaces acting as perfect electric conductors (PEC), where $Z_s = 0$ which corresponds to surfaces at the planes of zero intensity vector. On the contrary, surfaces with the behavior of perfect magnetic conductor (PMC) characterized by $Z_s = \infty$ are located at the planes of the maximum intensity vector.

C. Anomalous reflection

The third and the most interesting and general case is lossless reflection of a plane wave into an arbitrary direction, where in general both amplitudes and propagation directions are different: $|p_i| \neq |p_r|$, $(\mathbf{k}_r \neq \mathbf{k}_i)$. This scenario is known as anomalous reflection. For flat metasurfaces laying in the xz -plane, it was demonstrated that the relation between the incident and the reflected amplitudes is given by $R = |p_r|/|p_i| = \sqrt{\cos\theta_i/\cos\theta_r}$.

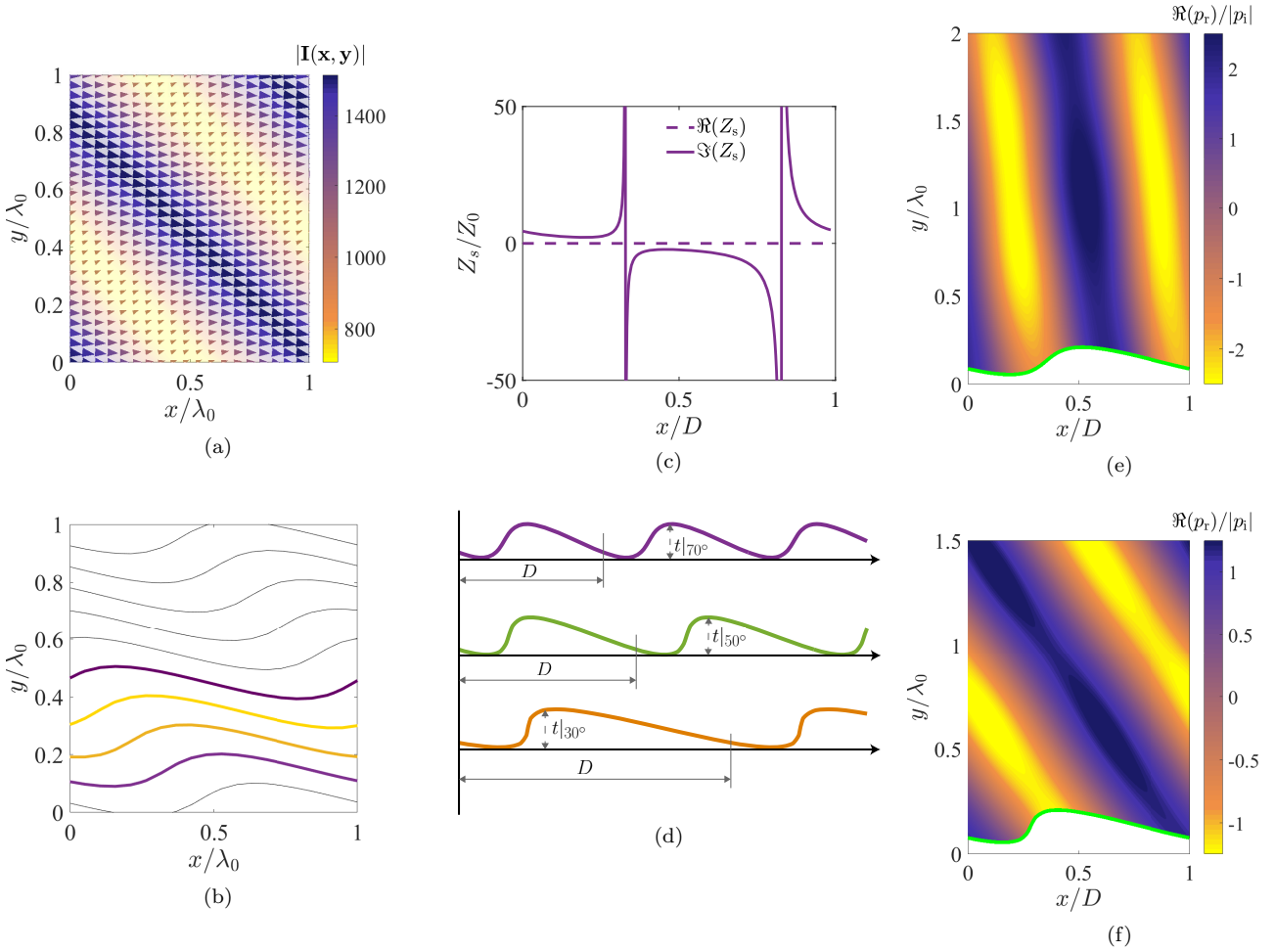


FIG. 4. Power flow-conformal metamirror for acoustic anomalous reflectors. (a) Power-flow distribution for $\theta_i = 0^\circ$ and $\theta_r = 80^\circ$. (b) Surface profiles for anomalous reflection when $\theta_r = 80^\circ$. (c) Surface impedance when $\theta_i = 0^\circ$ and $\theta_r = 80^\circ$. (d) Surface profiles for $\theta_i = 0^\circ$ and $\theta_r = 30^\circ, 50^\circ,$ and 70° . (e) and (f) Numerical simulations for $\theta_i = 0^\circ$ and $\theta_r = 80^\circ$ and $\theta_i = 0^\circ$ and $\theta_r = 70^\circ$.

The power flow distribution for the case of $\theta_i = 0^\circ$ and $\theta_r = 80^\circ$ is shown in Fig. 8(d).

As it was proposed in [12], instead of trying to synthesize flat surfaces with the required complex-valued impedances, we can create the desired field distribution shaping an impenetrable lossless reflector along surfaces which are tangential to the intensity vector. These surfaces can be found using the scalar function

$$g(x, y) = Ay + B \sin(\Delta \mathbf{k} \cdot \mathbf{r} + \Delta \phi) + C, \quad (6)$$

where $A = I_0 |p_i|^2 k_0 (\sin \theta_i + \cos \theta_i \tan \theta_r)$, $B = I_0 |p_i| \sqrt{\cos \theta_i / \cos \theta_r} (\cos \theta_i - \cos \theta_r) / (\sin \theta_r - \sin \theta_i)$, and C is an arbitrary constant. This scalar function satisfies $\nabla g(x, y) = \mathbf{N}(x, y)$, with vector $\mathbf{N}(x, y) = -I_y(x, y) \hat{\mathbf{x}} + I_x(x, y) \hat{\mathbf{y}}$ being orthogonal to the intensity vector. From the properties of the gradient, the surfaces tangential to the power flow directions can be calculated as the level curves of the function $g(x, y)$ and can be expressed as $y_c = f(x)$.

Probably the most studied case in the literature of anomalous reflection in a normally incident plane wave ($\theta_i = 0$) that is redirected into an arbitrary direction ($\theta_r \neq 0$). In this case, the surface profile and the surface impedance are different for each specific angle of reflection. Figure 4(d) shows the shapes of the perfectly anomalously reflecting surfaces for $\theta_r = 30^\circ, 50^\circ,$ and 70° . As can be expected, the period of the surface modulation changes with the reflected angle according to $D = \lambda / (\sin \theta_r - \sin \theta_i)$. The amplitude of the modulation, h , keeps almost constant for different incident angles ($h|_{30^\circ} = 0.1566\lambda$, $h|_{50^\circ} = 0.1538\lambda$, and $h|_{70^\circ} = 0.1386\lambda$), and is always subwavelength. The required surface impedances for these particular surfaces are plotted in Fig. 2(d). Two numerically simulated examples are presented in Figs. 2(c) and 2(d).

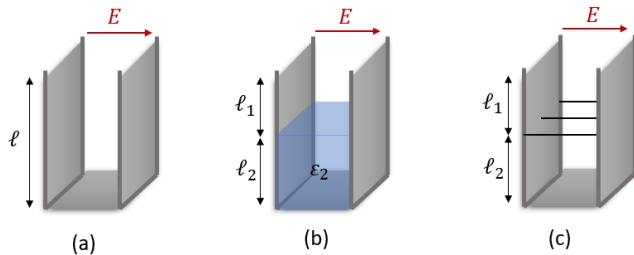


FIG. 5. Multiphysics meta-atoms. (a) Empty closed-end groves. (b) Partially filled closed-end groves. (c) Closed-end groves with a metallic grid.

III. MULTIPHYSICS IMPLEMENTATION

Here, we will show that using the concept of power flow-conformal metamirrors and the analogy between acoustic and electromagnetic impedances it is possible to create metasurfaces which operate as retro- and most general anomalous reflectors simultaneously for both acoustic and electromagnetic waves.

As it was explained above, the metamirrors functionalities are defined by the surface profile and the surface impedance. First, if we want to control both acoustic and electromagnetic waves, we need to ensure that the surface profiles required for both operations are compatible. In the previous section, we saw that some scenarios, such as anomalous reflection, require specific surface profiles. However, in other cases there is no such restriction and one can use different surface profiles for the same functionality, like for realizing retroreflectors. With this on mind, we distinguish two different design approaches: (i) Platforms that implement the same functionality for acoustic and electromagnetic waves and (ii) Platforms with different functionalities for acoustic and electromagnetic waves.

The second consideration is the design of the meta-atoms for implementing the corresponding surface impedance. Power flow-conformal metamirrors are described by locally defined acoustic or electromagnetic surface impedances, which allows implementations using conventional phase shifters of different types. The main challenge in the multiphysics realizations is to find such meta-atom configurations which will provide desired phase shifts both for sound and electromagnetic waves. We have identified three different structures which can be used for achieving this goal. The choice between them will be made based on specific conditions in each design. The schematic representations of the proposed three topologies are shown in Fig. 5.

The first meta-atom is a closed-end groove [see Fig. 5(a)]. Since here we consider surfaces which are modulated only along one direction, we assume that the groves are infinitely long and uniform. In general, two-dimensional arrays or tubes can be used. If the thickness of the walls is much smaller than the width of the groves, we can neglect the effect of wall thickness on the surface impedance.

The acoustic surface impedance $Z_s^{\text{ac}} = -jZ_0^{\text{ac}} \cot(k_{\text{ac}}\ell)$ is controlled by the depth of the groves ℓ and the acoustic impedance $Z_0^{\text{ac}} = c_{\text{ac}}\rho$ of air filling the tube. Here, $k_{\text{ac}} = 2\pi f_{\text{ac}}/c_{\text{ac}}$ is the acoustic wavenumber. For TE-polarized electromagnetic waves (electric field parallel to the groove), in the microwave range an array of groves reflects as a practically perfectly conducting surface (PEC) if the walls are made of metal and the width of the groves is deeply subwavelength. For TM-polarized electromagnetic waves, the response of the meta-atom is defined by the surface impedance $Z_s^{\text{EM}} = jZ_0^{\text{EM}} \tan(k_{\text{EM}}\ell)$, with $Z_0^{\text{EM}} = \sqrt{\mu_0/\epsilon_0}$ and $k_{\text{EM}} = 2\pi f_{\text{EM}}/c_{\text{EM}}$ being the electromagnetic wave impedance and the wavenumber in air, respectively.

The second proposed topology is the same closed-end groove but partially filled with a dielectric material with permittivity ϵ_2 . The dielectric material should be chosen to behave as a hard boundary for acoustic waves, introducing strong impedance contrast with air for acoustic waves. In practice, one can consider solid plastics or water. As we can see in Fig. 5(b), the filling with length ℓ_2 is placed at the bottom of the groove. The length of the air layer is denoted as ℓ_1 . The acoustic response of this meta-atom is defined by $Z_s^{\text{ac}} = -jZ_0^{\text{ac}} \cot(k_{\text{ac}}\ell_1)$. In contrast, the electromagnetic response for TM-polarized waves is given by the following surface impedance:

$$Z_s^{\text{EM}} = jZ_0^{\text{EM}} \frac{\tan(k_{\text{EM}}^{(2)}\ell_2) + \tan(k_{\text{EM}}\ell_1)}{1 - \tan(k_{\text{EM}}^{(2)}\ell_2) \tan(k_{\text{EM}}\ell_1)}. \quad (7)$$

Thus, the use of this structure allows us to independently tune both acoustic and electromagnetic impedances to the required values.

The third proposed topology is shown in Fig. 5(c). In this case, we use a groove of the total depth $\ell = \ell_1 + \ell_2$ with an array of metal wires oriented in the same direction as the electric field of TM-polarized waves and positioned at distance ℓ_2 from the bottom of the groove. The array of metal wires has a period d_w small enough for the array to act as a nearly perfect electric wall for electromagnetic waves. The reflection of electromagnetic waves is very strong when the period of the array of wires is much smaller than the wavelength of electromagnetic waves, while the diameter of the wires is still very small compared with the period [16]. This property allows us to realize a wire array which is nearly perfectly transparent for sound. The electromagnetic response of this meta-atoms is characterized by the surface impedance $Z_s^{\text{EM}} = jZ_0^{\text{EM}} \tan(k_{\text{EM}}\ell_1)$ while the acoustic response is defined by $Z_s^{\text{ac}} = -jZ_0^{\text{ac}} \cot(k_{\text{ac}}\ell)$. Again we see that there is a possibility to adjust both impedances independently.

Using these meta-atoms we can systematically design various devices for simultaneous control of electromagnetic and acoustic waves.

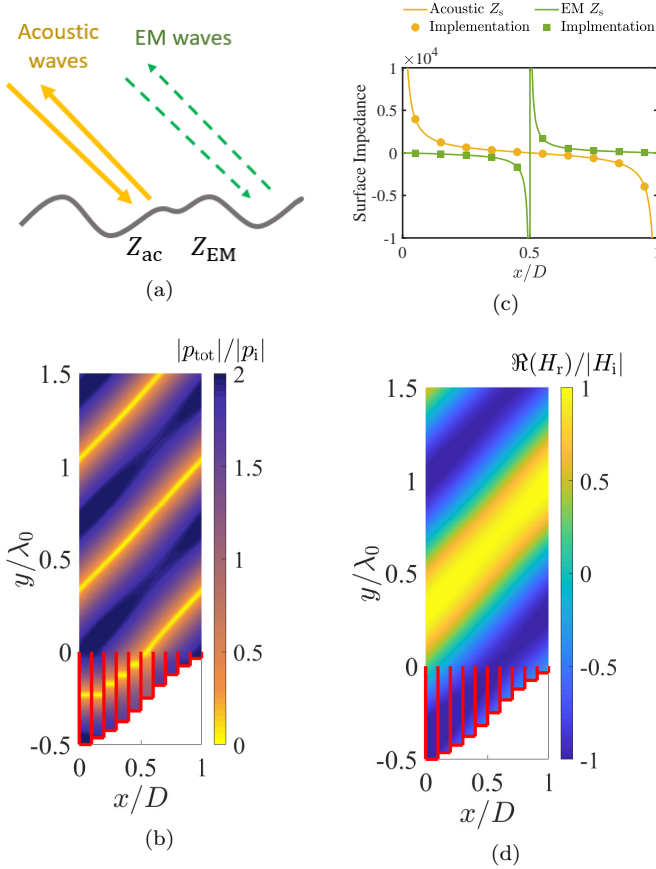


FIG. 6. Dual-physics retroreflector. (a) Schematic representation of the metamirror. (b) Total pressure field calculated with a numerical simulation for acoustic waves. Red lines denote the hard boundary conditions used for simulating the groves. (c) Surface impedance for electromagnetic (EM) and acoustic metamirror. (d) Reflected magnetic field calculated with a numerical simulation for EM waves. Red lines denote the PEC boundary conditions used for simulating the groves.

A. The same functionality in one platform

Here we explore possibilities to implement metamirrors with the same functionality for both electromagnetic and acoustic waves. In particular, we will use the proposed meta-atoms to implement dual-physics retroreflectors and anomalous reflectors.

Dual-physics retroreflector: Retroreflectors are able to send all the incident energy back into the same direction from where the incident wave is coming [see Fig. 6(a)]. Following the design methodology explained above, we will design a retroreflector working for acoustic and TM -polarized electromagnetic waves. The first step in the design of the multidisciplinary retroreflectors is to choose an appropriate reflector profile. In this work, for simplicity we use the simplest surface profile: a flat surface located in the xz -plane. As shown above, this is possible because the desired field structure is a purely standing wave without any power flow across any surface.

Once the retroreflecting surface position is defined, the periodicity is fixed by the operation frequencies, both in acoustics, f_{ac} , and in electromagnetism, f_{EM} . We start from considering the simplest case when the frequencies are such that $\lambda_{ac} = \lambda_{EM}$, i.e., the periodicity for both electromagnetic and acoustic scenarios is the same ($D_{ac} = D_{EM}$). To satisfy this condition, the frequencies should be related as $f_{EM} = f_{ac}c_{EM}/c_{ac}$. As an example, we assume that the background medium is air characterized by $c_{EM} = 3 \cdot 10^8$ m/s and $c_{ac} = 343$ m/s (the speed of sound in the background media has been calculated using a reference temperature of $T = 20^\circ\text{C}$).

The last step in the design is to implement the required surface impedances. For flat retroreflectors, the required surface impedances for electromagnetic and acoustic waves can be written as

$$Z_s^{ac}(x) = j \frac{Z_0^{ac}}{\cos \theta_i} \cot(k_{ac} \sin \theta_i x) \quad (8)$$

$$Z_s^{EM}(x) = -j Z_0^{EM} \cos \theta_i \tan(k_{ac} \sin \theta_i x) \quad (9)$$

The surface impedance values when $\theta_i = 70^\circ$ are represented in Fig 6(c). These surface impedance profiles can be implemented using empty closed-end groves as meta-atoms. The depths of the groves are 50 mm, 46.4 mm, 42.4 mm, 37.7 mm, 31.9 mm, 25 mm, 18.1 mm, 12.3 mm, 7.6 mm, and 3.6 mm. Figures 6(b) and (d) show the results of numerical simulation of a multidisciplinary retroreflector for $f_{ac} = 3430$ Hz and $f_{EM} = 3$ GHz. From the distribution of the total acoustic field represented in Fig. 6(b) we can see how a standing waves is generated as a consequence of interference between incident and reflected waves. Figure 6(d) shows the reflected field in the electromagnetic scenario where we can see that all the energy is sent back along the propagation axis of the incident wave.

If the acoustic and electromagnetic frequencies are arbitrary, and the corresponding wavelengths are not equal, the required periodicity of the metasurface for each scenario will be different, $D_{ac} \neq D_{EM}$. In this case, we select the period of the structure to be equal to the least common multiple of the two periods. It is also important to notice in this general case the relation between the acoustic and electromagnetic surface impedances is not described by Eqs. (8) and (9). Thus, implementation with simple close-ended groves is not possible. In this case, we should use meta-atoms consisting of partially filled closed-end groves or closed-end groves with a metallic grid, which allow realizations of the required impedance profiles for both fields. Two examples on how to use these meta-atoms are given in Section III.B

Dual-physics anomalous reflector: The second example is an anomalous reflector for acoustic and electromagnetic waves. The schematic representation of the proposed metamirror is shown in Fig. 7(a). This device is able to send impinging acoustic and electromagnetic plane waves coming from a certain direction into an arbitrary direction. As it was explained in Section II, in this case there is a periodic power-flow distribution in

the xy -plane. Following the design procedure for power flow-conformal metamirrors, the first step is to define an appropriate surface profile for the desired incident angle θ_i and the desired reflection angle θ_r , ensuring that the power flow is always tangential to the reflecting surface. The second step in the design is to implement the required surface impedances for both acoustic and electromagnetic waves. In this case, we will follow a similar approach as in the previous example and exploit the fact that the normalized Z_{ac} is analogous to normalized Y_{TM} . As we have already demonstrated, using empty metallic close-ended groves we can realize a metasurface which the desired acoustical and electromagnetic properties. In particular, for an anomalous reflector with $\theta_i = 0^\circ$ and $\theta_r = 70^\circ$, the needed depths of the groves are 5.9 mm, 7.8 mm, 10 mm, 11.7 mm, 49.5 mm, 38.3 mm, 40.1 mm, 42.2 mm, 44.2 mm, 46 mm, 47.6 mm, 49.2 mm, 0.8 mm, 2.4 mm, and 4.1 mm (considering the frequencies $f_{EM} = 3$ GHz and $f_{ac} = 3430$ Hz as an example). Figures 7(b) and (d) show the scattered fields produced by the structure at the operation frequency for both acoustical and electromagnetic scenarios.

B. Different functionalities in the same platform

Previous examples have shown a possibility to exploit the local behavior of power flow-conformal metasurfaces and the direct analogy between acoustic and electromagnetic waves to implement multidisciplinary meta-devices that produce the same response for acoustic and electromagnetic waves. Next, we propose meta-devices realizing different transformations for acoustic and electromagnetic waves. As particular examples, we will study a retroreflector with different angles for acoustic and electromagnetic waves and an anomalous reflector for acoustic waves that behaves as a retroreflector for electromagnetic waves.

Multidisciplinary retroreflector for different angles:

Here, we propose an implementation of flat retroreflectors able to work at different angles for acoustics and electromagnetic waves. The incident angle of electromagnetic illumination, θ_{EM} , will determine the periodicity for electromagnetic waves $D_{EM} = \lambda_{EM}/2 \sin \theta_{EM}$. Then, we define the periodicity for acoustic waves to be m -times bigger than the periodicity for electromagnetic waves $D_{ac} = \lambda_{ac}/2 \sin \theta_{ac} = mD_{EM}$. Free choice of the coefficient m allows us to control the operating incident angle for acoustic waves as $\theta_{ac} = \arcsin(\lambda_{ac} \sin \theta_{EM}/m\lambda_{EM})$. In our example, we will assume that $\lambda_{ac} = \lambda_{EM}$ by choosing the operation frequencies equal to $f_{EM} = 3$ GHz and $f_{ac} = 3430$ Hz. As another example, if we choose $m = 2$ and $\theta_{EM} = 80^\circ$, then $\theta_{ac} = \arcsin(\sin \theta_{EM}/2) = 29.5^\circ$.

The next step in the design is to implement the required surface impedance for both acoustic and electromagnetic scenarios, see Fig. 9(c). The main difference with the previous examples is that in this case there is no relation between the acoustic and electromag-

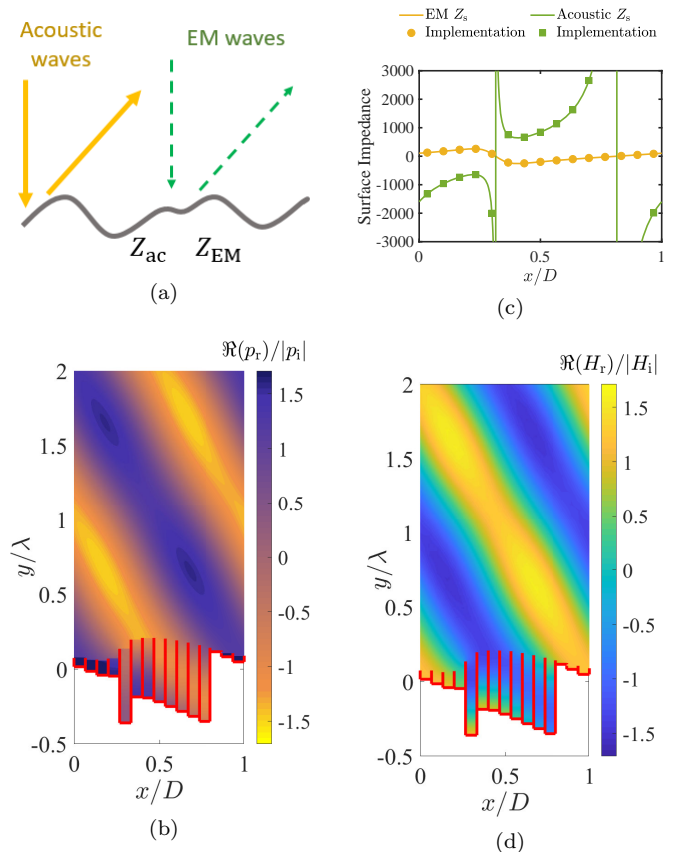


FIG. 7. Dual-physics anomalous reflector. (a) Schematic representation of the metamirror. (b) Reflected pressure field calculated with a numerical simulation for acoustic waves. Red lines denote the hard boundary conditions used for simulating the groves. (c) Surface impedances for electromagnetic (EM) and acoustic metamirror. (d) Reflected magnetic field calculated with a numerical simulation for EM waves. Red lines denote the PEC boundary conditions used for simulating the groove walls.

netic surface impedances. For this reason, we need to use meta-atoms that offer independent control of both impedances. In this example, we choose partially filled close-ended groves as meta-atoms. We chose a material used for filling the tube with the relative permittivity $\epsilon_2 = 2$. To systematically design the meta-atoms, we start implementing the acoustic response according to $Z_s^{ac} = -jZ_0^{ac} \cot(k_{ac}\ell_1)$. The depths of the empty volume of each grove, ℓ_1 , equal 48.5 mm, 45.6 mm, 42.6 mm, 39.4 mm, 36.1 mm, 32.5 mm, 28.8 mm, 25 mm, 21.2 mm, 17.5 mm, 13.9 mm, 10.6 mm, 7.4 mm, 4.4 mm, and 1.5 mm. Using Eq. (7) we can calculate the required length of the dielectric filling ℓ_2 . The found values of ℓ_2 are 0.6 mm, 1.7 mm, 2 mm, 31.3 mm, 15.4 mm, 14.5 mm, 15.9 mm, 17.7 mm, 19.5 mm, 20.9 mm, 20 mm, 4.1 mm, 33.4 mm, 33.7 mm, and 34.7 mm. In Fig. 9(b), a comparison between the required surface impedances and the impedances implemented with the actual meta-atoms is presented. Figures 9(c) and (d) show the results of a

numerical simulation of the structure response for acoustic and electromagnetic waves where we can see standing waves generated by the incident and reflected waves, with different operational angles for acoustic and electromagnetic waves.

Acoustic anomalous reflector and EM retroreflector:

In this last example, we propose and study a device that acts as a retroreflector for electromagnetic waves and as an anomalous reflector for acoustic waves. Since the electromagnetic retroreflector can be implemented with any surface profile, we start the design with the definition of the tangential to the power flow surface for the acoustic anomalous reflector. Using the theoretical approach described in Section IIC, we find the surface profile, $y_c = f(x)$, and calculate the surface acoustic impedance Z_s^{ac} . For the incident angle $\theta_i^{\text{ac}} = 0^\circ$ and the reflected angle $\theta_r^{\text{ac}} = 60^\circ$, the acoustic impedance is represented in Fig. 9(c). In this example, for the sake of simplicity, we chose the incident angle of the electro-

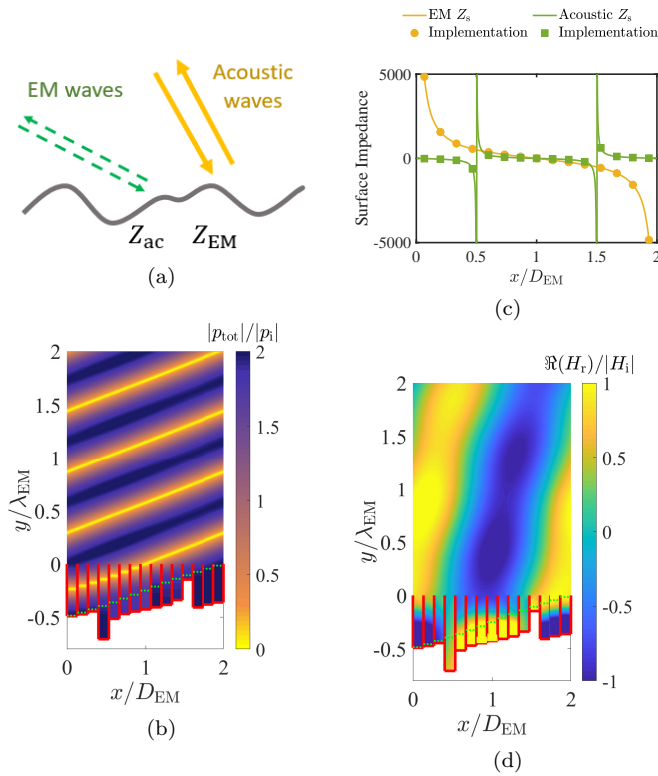


FIG. 8. Multidisciplinary retroreflector for different angles. (a) Schematic representation of the metamirror. (b) Total pressure field calculated with a numerical simulation for acoustic waves. Red lines denote the hard boundary conditions used for simulating the groves. Green dotted lines represent the transition between empty grove and the solid material. (c) Surface impedance for electromagnetic (EM) and acoustic metamirrors. (d) Reflected magnetic field calculated with a numerical simulation for EM waves. Red lines denote the PEC boundary conditions used for simulating the grove walls. Green dotted lines represent the transition between empty grove volume and the filling dielectric material.

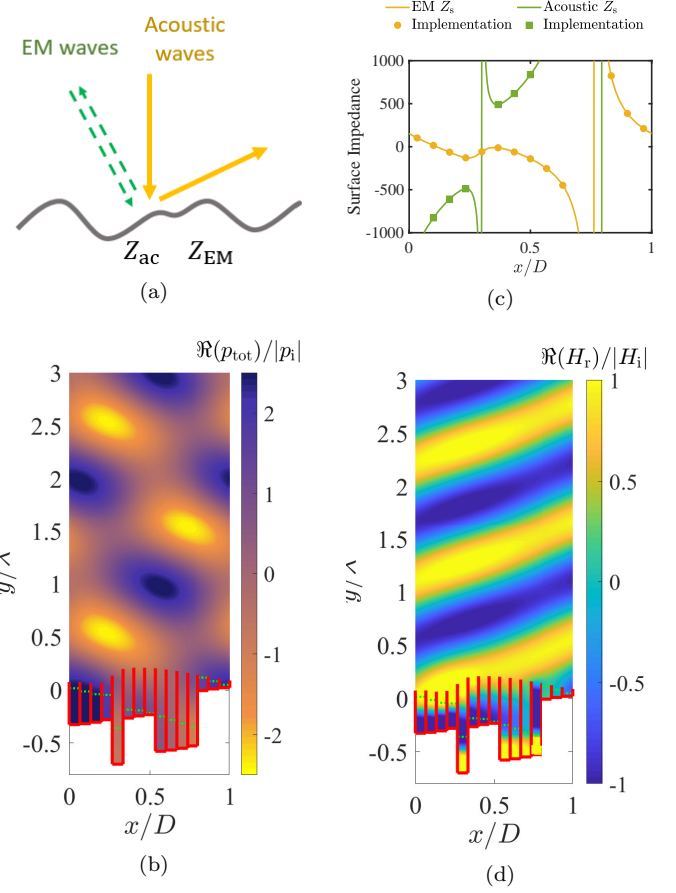


FIG. 9. Acoustic anomalous reflector and electromagnetic retroreflector. (a) Schematic representation of the metamirror. (b) Total pressure field calculated with a numerical simulation for acoustic waves. Red lines show the hard boundary conditions used for simulating the groves. Green dotted lines indicate the transition between empty grove volume and the solid filling material. (c) Surface impedance for electromagnetic (EM) and acoustic metamirrors. (d) Reflected magnetic field calculated with a numerical simulation for EM waves. Red lines denote the PEC boundaries used for simulating the grove walls. Green dotted lines represent the transition between empty grove volume and the dielectric filling material.

magnetic retroreflector, θ_i^{EM} , that corresponds to the same surface period as the acoustic anomalous reflector, $D_{\text{ac}} = D_{\text{EM}}$. Choosing the operation frequencies equal to $f_{\text{EM}} = 3$ GHz and $f_{\text{ac}} = 3430$ Hz, the angle of incidence for the electromagnetic retroreflector is $\theta_i^{\text{EM}} = 25.65^\circ$. The electromagnetic surface impedance Z_s^{EM} for the surface profile defined by y_c is represented in Fig. 9(c). As it was mentioned before, if the electromagnetic and acoustic periods are not equal, the period of the structure is chosen as their least common multiple.

Finally, once we know a suitable surface profile and the corresponding surface impedances, we design meta-atoms that implement the surface impedance for both scenarios. Because this device requires independent control of electromagnetic and acoustic impedances, we choose

as meta-atoms close-ended groves partially filled with a dielectric with relative permittivity $\varepsilon_2 = 2$. Using the analytical formulas presented at the beginning of this section, the lengths of the empty portion of the groves, ℓ_1 , that produce the desired acoustic response will be 5.9 mm, 7.8 mm, 10 mm, 11.7 mm, 49.5 mm, 38.3 mm, 40.1 mm, 42.2 mm, 44.2 mm, 46 mm, 47.6 mm, 49.2 mm, 0.8 mm, 2.4 mm, and 4.1 mm. Then, using Eq. (7), we calculate the required lengths of the dielectric filling ℓ_2 . The found values of ℓ_2 are 34.2 mm, 30.3 mm, 26.4 mm, 23.4 mm, 34 mm, 7.9 mm, 5.2 mm, 1.5 mm, 32.8 mm, 28.4 mm, 23.4 mm, 17.8 mm, 12.3 mm, 7.3 mm, and 2.8 mm. Figures 9(b) and 9(d) show the results of numerical simulations for acoustic and electromagnetic waves. In Fig. 9(b), the total acoustic field is represented and we can recognize the typical interference pattern generated by the incident wave and the reflected wave. Figure 9(d) shows the reflected magnetic field where we can see that the energy is sent back into the illumination direction.

IV. CONCLUSIONS

Multidisciplinary analysis of power flow-conformal metamirrors has been performed from both acoustic and electromagnetic points of view. Based on the revealed

analogy we have found a possibility to create metamirrors which operate as various anomalous reflectors both for electromagnetic and acoustic waves at the same time. We propose three simple meta-atom topologies that allow us to engineer and control the electromagnetic and the acoustic responses at will. The considered example functionalities include high-efficient (theoretically perfect) retroreflection and anomalous reflection for both waves. The theory and design approach can be expanded to more complex transformations such as, for instance, beam splitters for waves of one nature and retroreflectors for waves of the other nature. Thanks to the analytical formulation, the design process is straightforward and numerical optimizations are not required. This multidisciplinary approach opens a path for the design of multiphysics devices that integrate functionalities for both waves. Finally we note that the proposed topology of dual-physics meta-atoms allow electrical tunability, for example, using switches to control metal wire grids or using tunable materials as filling for the groves or tubes.

ACKNOWLEDGMENT

This work received funding from the the Academy of Finland under the grant project 309421.

-
- [1] B. Assouar, B. Liang, Y. Wu, Y. Li, J.-C. Cheng, and Y. Jing, *Nature Reviews Materials* **3**, 460 (2018).
 - [2] S. Glybovski, S. Tretyakov, P. Belov, Y. Kivshar, and C. Simovski, *Physics Reports* **634**, 1 (2016).
 - [3] O. Quevedo-Teruel, *Journal of Optics* **21** (2019).
 - [4] N. Estakhri and A. Alu, *Physical Review X* **6**, 041008 (2016).
 - [5] A. Díaz-Rubio, V. Asadchy, A. Elsakka, and S. Tretyakov, *Science Advances* **3**, e1602714 (2017).
 - [6] A. Epstein and O. Rabinovich, *Physical Review Applied* **8**, 054037 (2017).
 - [7] Y. Radi, D. L. Sounas, and A. Alu, *Physical Review Letters* **119** (2018).
 - [8] D. Kwon, *IEEE Antennas and Wireless Propagation Letters* **17** (2018).
 - [9] V. Asadchy, A. Díaz-Rubio, S. Tsvetkova, D. Kwon, A. Elsakka, M. Albooyeh, and S. Tretyakov, **7 3** (2017).
 - [10] A. Díaz-Rubio and S. Tretyakov, *Physical Review B* **96**, 125409 (2017).
 - [11] D. Torrent, *Physical Review B* **98**, 060101(R) (2018).
 - [12] A. Díaz-Rubio, J. Li, C. Shen, S. Cummer, and S. Tretyakov, *Science Advances* **5**, eaau7288 (2019).
 - [13] C. Shen, A. Díaz-Rubio, J. Li, and S. Cummer, *Applied Physics Letters* **112**, 183503 (2018).
 - [14] V. Popov, F. Boust, and S. N. Burokur, *Physical Review Applied* **10**, 011002 (2018).
 - [15] J. Carbonell, D. Torrent, A. Díaz-Rubio, and J. Sánchez-Dehesa, *New Journal of Physics* **13**, 103034 (2011).
 - [16] S. Tretyakov, *Analytical Modeling in Applied Electromagnetics* (Norwood, MA: Artech House, 2003).